Earth Planets Space, **63**, 941–948, 2011

Effects of solar cycle variations on oxygen green line emission rate over Kiso, Japan

Uma Das[1], C. J. Pan[1], and H. S. S. Sinha[2]

[1]*Institute of Space Science, National Central University, Jhongli—32001, Taiwan*
[2]*Physical Research Laboratory, Ahmedabad—380009, India*

(Received October 4, 2010; Revised April 12, 2011; Accepted April 19, 2011; Online published December 29, 2011)

A sixteen year long dataset of mesospheric OI 557.7 nm green line nightglow emission rate, measured over Kiso (35.79°N, 137.63°E), Japan using ground-based photometers is spectrally investigated using the Hilbert-Huang Transform (HHT). The spectrograms reveal the presence of semi-annual, annual and quasi-biennial oscillations in consonance with the results obtained from wavelet analysis in an earlier study. In addition, due to the use of the HHT, we have been able to investigate the very low frequency solar cycle variation in the emission rate. It is found that there is a signi cant solar cycle effect on the oxygen green line emission rate. The mean amplitude of variation is approximately 20% and it is also found that it is maximum at midnight. A correlation study between the means of the emission rate and the solar radio ux at 10.7 cm also shows that the effect of solar activity on the oxygen green line emission rate is maximum at midnight.
Key words: Mesosphere, airglow, Hilbert-Huang Transform, solar cycle effects.

1. Introduction

Oxygen green line airglow (OI 557.7 nm) emission rate is a unique parameter to understand the neutral dynamics of the 90–100 km region as the bulk of the emission comes from the mesopause and the lower thermosphere. There is also a contribution from the thermosphere over the equatorial and the equatorial ionization anomaly regions but not for mid-latitudes (Shepherd *et al*., 1997; Nicolls *et al*., 2006). The thermospheric contribution over the equator can exceed the mesospheric component during the post midnight hours of high solar activity period (Rajesh *et al*., 2007).

It is now well established that O(^{1}S), the source of green line emission, is the result of a two-step Barth mechanism (Barth and Hildebrandt, 1961; Barth, 1964), involving a three body recombination reaction, where the third body M can be O_2, N_2 or O.

$$\mathrm{O}\left(^3\mathrm{P}\right) + \mathrm{O}\left(^3\mathrm{P}\right) + M \rightarrow \mathrm{O}_2^* + M \quad (1)$$

$$\mathrm{O}_2^* + \mathrm{O}\left(^3\mathrm{P}\right) \rightarrow \mathrm{O}_2 + \mathrm{O}\left(^1\mathrm{S}\right) \quad (2)$$

$$\mathrm{O}\left(^1\mathrm{S}\right) \rightarrow \mathrm{O}\left(^1\mathrm{D}\right) + h\nu\ (\lambda = 557.7\ \mathrm{nm}) \quad (3)$$

Atomic oxygen is produced during the day by the photodissociation of molecular oxygen by absorption of solar radiation in the Schumann Runge continuum (135–175 nm) and the Schumann Runge bands (175–242 nm).

The green line airglow emanating from this atmospheric species has always been of immense interest and is still investigated to understand the mesosphere and the lower thermosphere (MLT) region.

There have been many ground-based and satellite-based studies in the past that addressed the short-and long-term variations of the oxygen green line emission (Brenton and Silverman, 1970; Donahue *et al*., 1973; Fukuyama, 1976, 1977; Cogger *et al*., 1981; Shepherd *et al*., 1995, 2005; Yee *et al*., 1997; Deutsch and Hernandez, 2003; Reid and Woithe, 2007; Das and Sinha, 2008; Liu and Shepherd, 2008; Liu *et al*., 2008a, b).

The diurnal variations observed were due to the tidal variations in the MLT region (Brenton and Silverman, 1970; Fukuyama, 1976; Shepherd *et al*., 1995, 1998; Liu *et al*., 2008a). Model results by Ward (1999) reinforced the role of tidal dynamics in the diurnal variation of the oxygen green line airglow. Fukuyama (1977) examined the seasonal and other long-term variations using ground-based measurements from a number of stations in the northern hemisphere. The most signi cant variation was the annual component with smaller amplitudes at low latitudes and larger amplitudes at higher latitudes. The next important oscillation was the semi-annual component, showing the opposite trend. It had maximum amplitude over the equator which decreased with increasing latitude. Deutsch and Hernandez (2003) also showed the same results with data from 29 stations covering both the northern and southern hemispheres. Liu and Shepherd (2008) studied the tropical O(^{1}S) nightglow variations using data from the Wind Imaging Interferometer (WINDII) instrument onboard the Upper Atmosphere Research Satellite (UARS) and ground-based photometers installed at Arecibo Observatory (18°N, 67°W) and found that both datasets exhibited semi-annual variation with maxima at the two equinoxes and minima at the solstices. Liu *et al*. (2008a) investigated the sea-

doi:10.5047/eps.2011.04.006

sonal variations in the O(^{1}S) and OH nightglow emission rates at mid-to-high latitudes using WINDII/UARS data and showed that both emissions showed semi-annual and annual variations at specific altitudes and local times. Vertical advection associated with tides and the large-scale circulation was found to play a major role in these airglow seasonal variations.

Deutsch and Hernandez (2003) have investigated in very great detail the oxygen green line observations from Kiso (35.79°N, 137.63°E), Japan available from 1979–1990. Periodogram analysis done in this work showed statistically significant annual and semi-annual components, with the annual component beginning as a not so significant component but at the end of twelve years, it appeared as the most significant feature of the spectrum. Later Das and Sinha (2008) showed by wavelet analysis using the same Kiso dataset, which was slightly longer (1979–1994), that the annual component was indeed weaker in the initial years from 1979–1982 and that during this period the semi-annual oscillation had dominated. In the former study, what had been observed was a cumulative effect of observed periodicities during the periods 1979–1982, 1979–1985, 1979–1988, 1979–1990 using the one-dimensional periodograms that led to the inferences. In the latter study, the use of the continuous wavelet transform had enabled the visualization of the time-frequency localisation and how the annual and semi-annual components varied through time was understood. The quasi-biennial oscillation also was identified using the wavelet analysis (Das and Sinha, 2008) and was not seen in the earlier study (Deutsch and Hernandez, 2003). Shiokawa and Kiyama (2000) also investigated the Kiso data (1979–1994) and found the presence of two seasonal peaks, one in June and the other in October, however, no detailed spectral analysis was performed. Reid and Woithe (2007) used a 11 year long database of oxygen green line nightglow observations over Buckland Park (34.9°S, 138.6°E), near Adelaide, Australia, a geographically conjugate station to Kiso, and found that the annual and semi-annual components were almost equal in amplitude and varied between 14–17% of the mean intensity. They also found a quasi-biennial component, with a smaller amplitude of 5% of the mean intensity.

The other important result obtained by Das and Sinha (2008) was that the semi-annual oscillation was very significant at 2000 hrs JST (Japan Standard Time) and as the night progressed, the amplitude of the oscillation reduced. This observation was possible because the nightglow observations at each hour had been considered separately, instead of using the nightly means as done in earlier studies. This result is in absolute conformity with the observations of WINDII/UARS and also the TIME-GCM (Thermosphere-Ionosphere-Mesosphere-Electrodynamics-Global Circulation Model) model calculations of the oxygen green nightglow (Shepherd *et al.*, 2005). The annual and the quasi-biennial oscillations, on the other hand, weakened towards midnight, and their amplitudes increased during the post-midnight hours. This local time dependence of the amplitudes of the long term periods is due to the effect of tides on the oxygen emission rates.

In addition to these long term periods, the oxygen emission rate is also influenced by the 11-year solar cycle (Deutsch and Hernandez, 2003; Liu *et al.*, 2008b; Liu and Shepherd, 2008). Deutsch and Hernandez (2003) observed that the emission rate increases with solar activity being higher during the decreasing phase of the solar activity, but this relationship varies slightly with different solar cycles. Liu *et al.* (2008b) also showed that the WINDII and the Arecibo datasets were consistent with the solar flux variation. Liu and Shepherd (2008) investigated the solar cycle impact on the green line emission rate specifically, and found that the latter was related linearly to the solar $F_{10.7\,\mathrm{cm}}$ flux, which is a good proxy for solar UV irradiance. The study of effect of solar cycle variation on the upper atmosphere at almost all times faces the problem of lack of sufficient length of data. Deutsch and Hernandez (2003) have shown in their study of the long term (annual and semi-annual) variations of the oxygen green line nightglow that to establish a statistically significant climatology of a periodicity, the data length should be at least 20 times the same. It is highly impossible to obtain such a long data series to study the solar cycle variations. Also, measurements would not be possible with the same instrument and/or human operator and thereby introduce errors, which require proper inter-calibrations and corrections. The Kiso nightglow data, is a valuable dataset presenting 16 year long observations of the oxygen green line nightglow emission rate from 1979, a solar maximum year, through 1989, the next solar maximum year, to 1994. The solar minima were during 1986 and 1996. The present study is a re-investigation of the Kiso data using the Hilbert Huang Transform (HHT)—a better spectral analysis tool in terms of extracting the low frequency components (Huang *et al.*, 1998; Huang and Wu, 2008)—to address the solar cycle variations and effects on the oxygen nightglow. Section 2 describes the Kiso data and Section 3 describes HHT in detail. The results from the analysis are discussed in Section 4.

2. Data

Nightglow measurements of column integrated OI 557.7 nm zenith emission rate observed using ground-based photometers at Kiso are taken from the World Data Center (WDC) C2 for Airglow, Tokyo, Japan. All measurements were made on moonless nights. Figure 1 shows a histogram

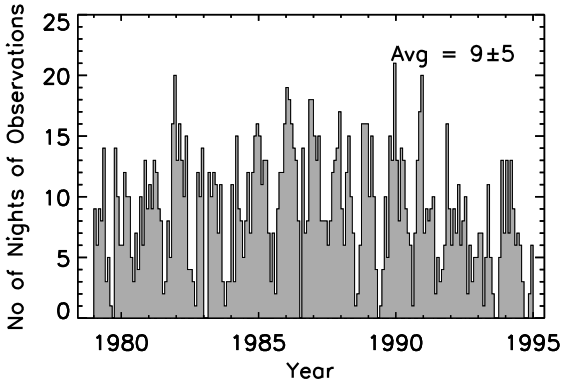

Fig. 1. Histogram showing the number of nights of observations per month of the oxygen green line emission rate during 1979–1994.

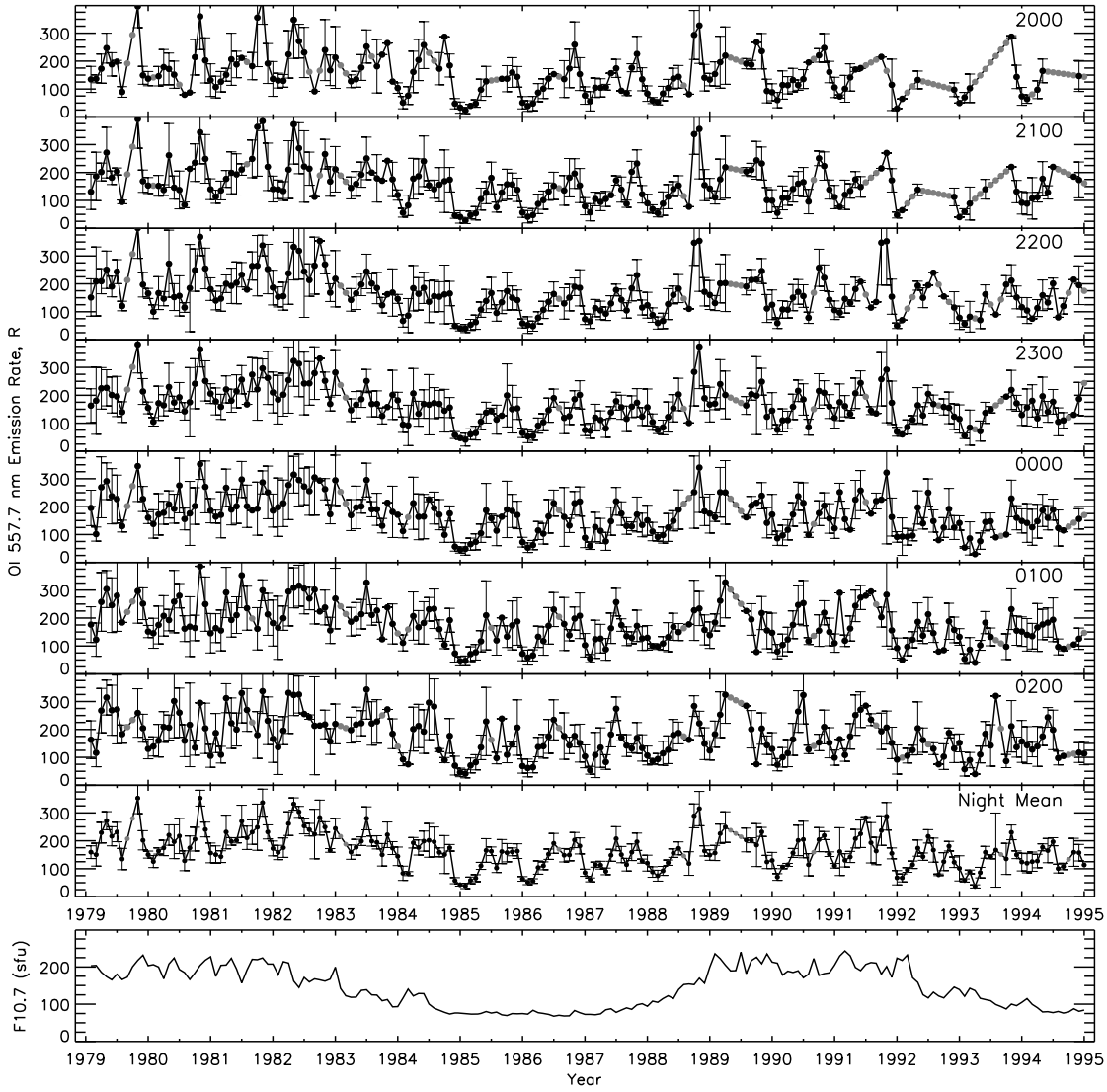

Fig. 2. Monthly averages of the oxygen green line emission rate at each hour of the night from 2000 to 0200 hrs JST, the nightly mean and the solar 10.7 cm radio flux during the study period.

of the number of observational nights per month during the period 1979 to 1994. The average number of observations for the 16 year long period is 9±5 nights per month. Data from 1979 to 1990 are available at one-minute intervals and hourly averages are computed from this data. From 1991 to 1994, hourly averages are provided by WDC and these data values are concatenated to the earlier computed averages, thus forming a 16 year long data set of hourly zenith emission rates of OI 557.7 nm green line nightglow. Monthly averages at each hour of the night are then computed to investigate the long term behavior in the nightglow emission rates. By treating the hourly averages separately, the data consists of twelve time series starting from 1800 hrs JST (Japan Standard Time) to 0500 hrs JST. However, observations at 1800, 1900, 0300, 0400, and 0500 hrs JST are very sparse and therefore are not included in the present study. The focus is on the more continuous series from 2000 hrs, through midnight, to 0200 hrs JST. These monthly average emission rates at each hour are shown in Fig. 2. The black filled circles are the averages, and the red filled circles are interpolated points, where data is not available. Interpolation has to be done due to the requirement of the spectral analysis technique that the data should be equally spaced. The penultimate panel of the figure shows the monthly nightly mean emission rates. This has been included in the study to impress upon the results obtained by considering the monthly means at each hour. The last panel shows the monthly mean solar 10.7 cm radio flux, as a proxy for solar UV irradiance.

3. Hilbert-Huang Transform

Spectral analysis tools are very important in understanding the periodic variations of different parameters in observational sciences. The most popular until now is the Fourier transform, which is useful for spectral analysis of linear and stationary data. However, seldom are geophysical datasets linear and stationary. The wavelet transform provided an advancement as it is capable of analyzing non-stationary data and gives time-frequency localization (Farge, 1992; Torrence and Compo, 1998). It is still inadequate as it cannot handle non-linear data and also its non-local adaptive approach results in leakage giving the spectrum an

overly smoothed appearance. To address these problems, the Hilbert-Huang Transform, HHT, (Huang *et al.*, 1998; Huang and Wu, 2008) has been proposed, which is capable of dealing with non-stationary as well as non-linear data series and is described below. HHT consists of two main elements—(1) Empirical Mode Decomposition (EMD) of the source data into an adaptive basis called Intrinsic Mode Functions (IMFs) and (2) Hilbert spectral analysis of the IMFs to generate a time-frequency-energy representation. It is the first local and adaptive method in frequency-time analysis.

The EMD phase is an iterative process, where envelopes and their means of a data vector are used to break the latter into components called IMFs. In each iteration, the envelope mean is subtracted from the data vector. This is called the 'sifting' process and is repeated until an IMF is obtained. An IMF is defined as a function, (1) where the number of zero crossings and extrema are equal or differ at most by one; and (2) at any point, the mean value of the envelopes defined by local maxima and local minima is zero. Once the first IMF is obtained, it is subtracted from the original data vector and the remaining portion of the signal is subjected to the 'sifting process' to determine the second IMF and so on. The process continues until the last IMF or the residue is less than a predetermined value of substantial consequence, or when the residue becomes a monotonic function from which no more IMF can be extracted. Even for data with zero mean, the final residue can be different from zero; for data with a trend the final residue is the trend. If $X(t)$ is a time series and its IMFs are c_i, for $i = 1$ to n, and residue is r_n, then

$$X(t) = \sum_{i=1}^{n} c_i + r_n \tag{4}$$

Thus, the data is decomposed into n-empirical modes and a residue. The equation above shows the 'completeness' of the decomposition.

All IMFs are well-suited for the Hilbert transform which is defined as follows. For a time series, $c(t)$, the Hilbert transform, $H(t)$ is

$$H(t) = \frac{1}{\pi} P \int_{-\infty}^{\infty} \frac{c(t')}{t - t'} dt' \tag{5}$$

where P indicates the Cauchy principal value. With this definition, $c(t)$ and $H(t)$, form a complex conjugate pair, and so we can have an analytical signal $Z(t)$, as

$$Z(t) = c(t) + iH(t) = a(t)e^{i\theta(t)} \tag{6}$$

in which,

$$a(t) = \left[c^2(t) + H^2(t)\right]^{1/2}; \quad \theta(t) = \arctan\left(\frac{H(t)}{c(t)}\right) \tag{7}$$

Theoretically, there are infinitely many ways to define the imaginary part, but the Hilbert transform provides a unique way of defining so that the result is an analytic function. More discussion on this can be found in Bendat and Piersol (1986). The instantaneous frequency is then defined as

$$\omega = \frac{d\theta(t)}{dt} \tag{8}$$

The concept of instantaneous frequency is controversial and a discussion on the aspect is beyond the scope of the present study. Further details can be found in Huang *et al.* (1998) and references therein. After ω is computed, the data can be expressed as follows.

$$X(t) = \sum_{j=1}^{n} a_j(t) \ \exp\left(i \int \omega_j(t) dt\right) \tag{9}$$

It is very interesting to note that this is a generalized form of the Fourier transform. We can then represent the amplitude and instantaneous frequency, which are functions of time, in a three dimensional plot, in which the amplitude is contoured in a time-frequency plane. It is called the Hilbert spectrum, $H(\omega, t)$. The strength of this method lies in the fact that the basis of the decomposition is derived and defined *a posteriori* from the data and most importantly, the data is used most efficiently in this process. All data is used to define the longest period component. Furthermore, we do not need a whole wave to define the local frequency, for the Hilbert transform gives the best fit local sine or cosine form to the local data (Eq. (5)) and the frequency resolution at any point is uniformly defined by the local derivative of the phase (Eq. (8)). This is especially effective in extracting the low-frequency oscillations.

We also define the marginal Hilbert spectrum, $h(\omega)$, from the Hilbert spectrum as follows.

$$h(\omega) = \int_0^T H(\omega, t) dt \tag{10}$$

It is an analogy for the Fourier spectrum and the global power spectrum of wavelet analysis.

4. Results and Discussion

A 16-year climatological average of the green line emission rate is shown in Fig. 3 as a function of month and time of the night. Observe that during January the emission rates are minimum and are maximum during June and October in general, similar to that seen by Shiokawa and Kiyama (2000). Also, during the winter months, the emission rate is increasing as the night progresses, with a maximum at midnight and decreasing during post midnight hours. During March to August i.e., during spring equinox and summer, there is an increasing trend in the emission rate as the night progresses and the opposite is seen during September to October i.e., during vernal equinox, where the emission rate is showing a decreasing trend. We know that the green line emission is greatly influenced by the dynamical processes, especially the tides (Shepherd *et al.*, 1995, 1999; Ward, 1999). Generally, a minimum is seen during midnight over the equator, while the mid-latitudes experience a maximum. The observed climatology in the present study proves this aspect that the tides have a great influence on the nightglow emission and in addition, they also show that the effect is also a function of season.

The OI 557.7 nm green line emission rates at each hour and the nightly mean emission rate are analysed using the HHT. Figure 4 shows the decomposition of the nightly mean emission rate into five IMFs and a residue. A frequency component in the data series at an instant appears in

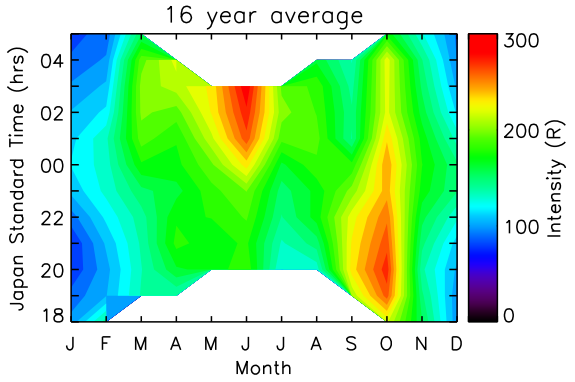

Fig. 3. A 16-year climatological monthly average of the oxygen green line emission rate at each hour of the night.

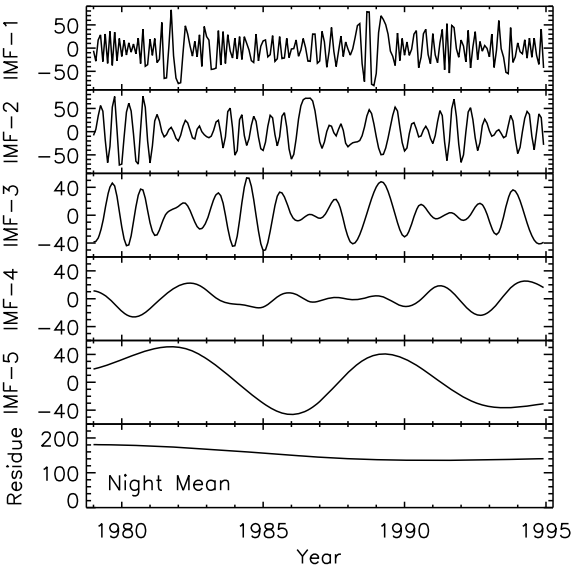

Fig. 4. The IMFs of the nightly mean emission rate. The residue is shown in the bottom panel.

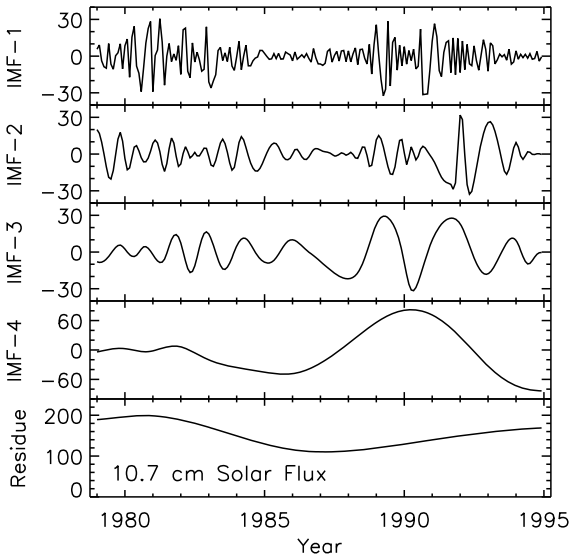

Fig. 5. Same as Fig. 4, but for the solar 10.7 cm radio flux.

one of the IMFs and it is not necessary that information regarding a frequency component appear in the same IMF at all times. In Fig. 4, one can see that the high frequency components are present in IMF-1, semi-annual components appear mostly in IMF-2, annual component in IMF-3 and the quasi-biennial component in IMF-4. IMF-5 shows a much higher periodicity, similar to (i.e., in phase with) the solar cycle variation and the amplitude of variation is approximately ±40 R, i.e., ∼20 % of the mean emission rate. The amplitudes of variation of the emission rates at each hour of the night at this period are also of the same order varying between 15 to 30%, with specific local time dependence. The residue in the last panel of the figure shows that there is a definite decreasing trend in the green line emission rate. It is also possible that this trend is a part of a much longer period of variation—longer than the length of the data. Figure 5 shows a similar decomposition of the monthly mean solar radio flux at 10.7 cm. The high frequency components are present in IMF-1 and it can be seen that the amplitudes of these components are high during the high solar activity periods. Lower frequencies are seen in successive IMFs. The 11 year solar cycle variation can be seen in IMF-4 and in the residue. It should be noted that the solar cycle period is not exactly 11 years and it is also not symmetric (last panel of Fig. 2). The decreasing phase from the solar maximum in 1979 to the minimum in 1986 was for 7 years and the next maximum was reached in 3 years by 1989. It later started decreasing to reach minimum in 1996.

Figure 6 shows a comparison of the trends/residues obtained from all the series. The mean emission rate and the emission rates at most of the times show a decreasing trend up to 1990 and a small increasing trend later. At 2100 and 2200 hrs, the decreasing trend is seen up to 1987 and the increasing trend that follows is very significant. The trend in $F_{10.7\,\mathrm{cm}}$ solar flux, is similar to that at these times during the later half of the period of interest. During the initial few years, it is very different from the trends in the nightglow emission rates. This is probably due to a leakage of the solar cycle periodicity into the residue.

The Hilbert energy spectra computed from the IMFs of the nightglow data are shown in Fig. 7. The last spectrum is that of the 10.7 cm radio flux. The residues also have been included in the computation, but the spectra are truncated to a frequency less than the length of the dataset, which coincidentally is 10.7 years—very close to the solar cycle periodicity. The raw spectrum obtained from HHT looks like a skeleton, especially at high frequencies, with small islands of high power in the time-frequency space. The readers are referred to Huang *et al.* (1998) for further details regarding the raw spectrum and its comparison to wavelet spectrum. Smoothing of the raw spectrum is applied to make the high power peaks visible, but it degrades the time and the frequency resolutions and hence, an appropriate smoothing window is selected depending upon the aim of the study. Das and Sinha (2008) have discussed the semi-annual, annual and the quasi-biennial components in detail. Hence in the present study, we would like to check whether the same results are obtained using HHT and in addition, investigate the very low frequency components and trends in the data. By trial and error, we have thus chosen and

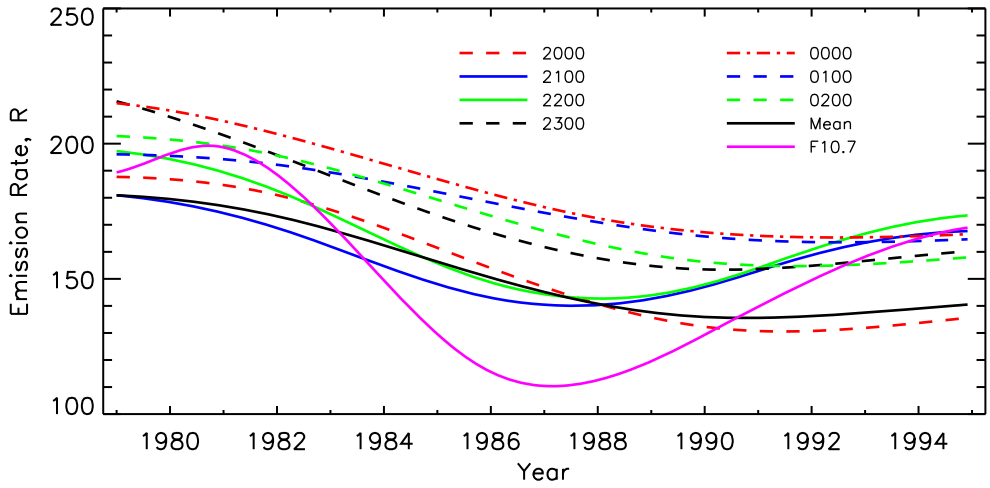

Fig. 6. The residues from the empirical mode decomposition of the oxygen green line emission rates from 2000 to 0200 hrs JST, the nightly mean and the solar 10.7 cm radio flux.

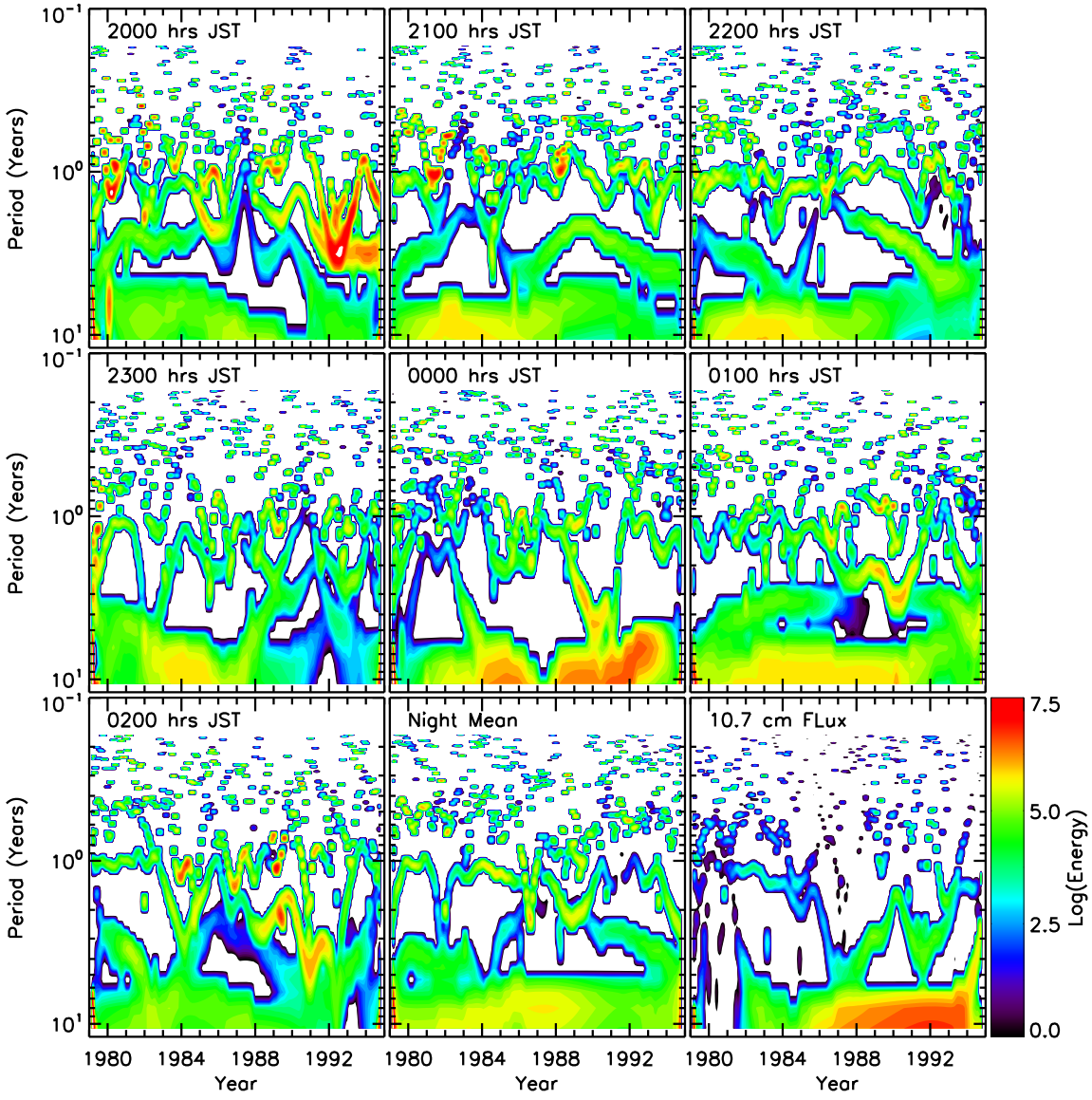

Fig. 7. The time-frequency-energy spectrograms obtained from the HHT analysis of the green line emission rate at each hour of the night from 2000 to 0200 hrs JST, the nightly mean and the solar 10.7 cm radio flux.

used a 5×5 Hanning window to smooth the raw Hilbert spectrum to better visualize the results. These spectra are visually different from the wavelet spectra obtained by Das and Sinha (2008), however, a closer look reveals that the results obtained by both methods are same. A semi-annual variation (0.5–0.6 years) can be seen at 2000 hrs during 1979–1982 and as the night progresses, the energy at this period reduces and almost disappears after midnight. The energies of the annual and the quasi-biennial oscillations, on the other hand, reduce from 2000 hrs JST to midnight and later start increasing once again. Figure 8 shows the marginal Hilbert spectrum from 2000 hrs to 0200 hrs JST, which confirms the above discussed results. Grid lines are also plotted in the figure to aid the eye at midnight along the time axis and at semi-annual, annual, quasi-biennial, and solar cycle periodicities along the period axis. It should be noted that the period corresponding to the length of the data is also included in the plot, and it contains overpowering energy associated with it (yellow).

The additional result obtained from the HHT analysis, which fulfills the aim of the present study, is as follows. A solar cycle variation at ∼11 years can be seen in Fig. 7 in the nightglow Hilbert spectra. The energy is high during the first half of the measurement period and increases from 2000 hrs JST to midnight. At midnight, the energy is high during almost all years. Later, it reduces once again by 0200 hrs JST. The nightly mean emission rate also shows the presence of the solar cycle periodicity. Interestingly, the $F_{10.7\,\mathrm{cm}}$ spectrum shows the 11 year variation during the second half of the measurement period. It is, as discussed earlier, probably due to the leakage of the solar cycle period into the residue during the initial few years. A close look at the monthly means in the last panel of Fig. 2 shows that there is no significant variation in the 10.7 cm flux apart from a small seasonal variation, resulting in almost 'no power' in the low frequency range during 1979–1982. Figure 8 also shows this local time dependence of the solar cycle period in the nightglow data. It can be seen that, the energy in the marginal Hilbert spectrum at 11 years is maximum at midnight. Figure 9 shows a correlation study of the mean emission rates with the mean solar 10.7 cm radio flux. At monthly and seasonal time scales, the correlation coefficients are poor and in the range of 0.3–0.5. The yearly means, however, show a good correlation ranging from 0.6 to 0.8. The important aspect to be noted here is that the effect of the solar activity seems to be highest at and around midnight at all temporal scales, similar to that observed from the HHT analysis. Correlation analysis of de-seasonalized WINDII data with $F_{10.7\,\mathrm{cm}}$ flux by Liu and Shepherd (2008) also showed that at 35°N, the correlation coefficient was 0.79. At other latitudes in the 40°S–40°N range also, the correlation coefficient was found to vary between 0.63 to 0.79, similar to that observed in the present study.

It is known that the atomic oxygen, from which the green line emission takes place, is produced from the photodissociation of molecular oxygen during the day in the 100–140 km region, and is a function of the solar energy inputs. Hence, when this atomic oxygen is carried down to mesopause levels during the night by tides, it carries with

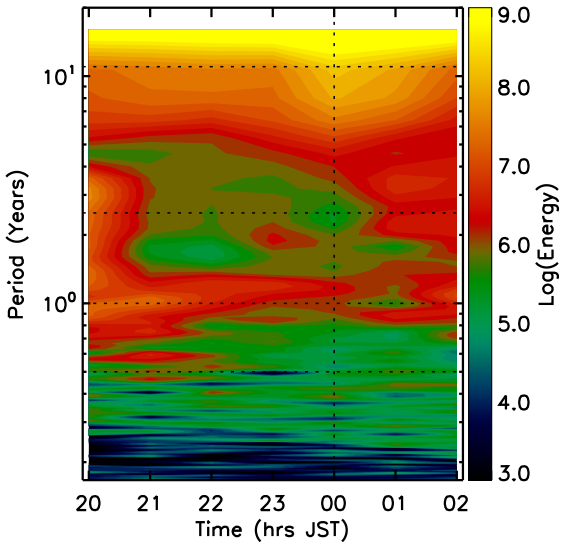

Fig. 8. The marginal Hilbert spectrum as a function of time of the night and period. Grid lines at semi-annual, annual, quasi-biennial, and solar cycle periodicities along the period axis, and at midnight along the time axis are shown to aid the eye.

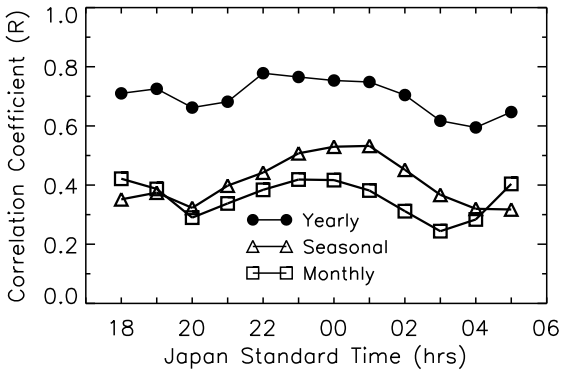

Fig. 9. A correlation study between the mean green line emission rate and the mean solar 10.7 cm radio flux at monthly, seasonal and yearly time scales.

it the imprint of the solar cycle effect. We thus observe the local time dependence in the solar cycle effect on the oxygen green line emission rate. This investigation once again establishes the important effects of tides and the large-scale circulation in the MLT region on the long term variations of the atomic oxygen and the green line emission rates, starting from seasonal variations to solar cycle variations.

5. Summary and Conclusions

We have analyzed 16 year long data of the oxygen green line emission rate over Kiso, Japan using the Hilbert Huang transform (HHT). The importance of this method lies in its efficiency to extract low frequency components by computing the instantaneous frequency. The approach of this method is local and adaptive as the basis set for the decomposition is derived from the data itself. By using this method, we have been able to identify the solar cycle variations in the emission rates and also the local time dependence of the solar cycle effects on the emission rates. We find that there is a significant effect of the solar cycle on the green line emission rate. The mean amplitude of variation

is ∼20% and is maximum at midnight. A correlation study between the means of the emission rates and the solar radio ux at 10.7 cm also shows that the effect of solar activity is maximum at and around midnight.

In addition to the investigation of the oxygen green line emission rates, this study also shows that HHT is a powerful spectral analysis tool which presents the time-frequency-energy spectrum of the data with very high temporal and spectral resolutions. It addresses and solves many problems faced with the traditional Fourier analysis and the currently well established and highly preferred wavelet transform. This method is very useful in investigating geophysical data that is most of the time non-local and non-stationary.

Acknowledgments. Authors thank the World Data Center C2 for Airglow (http://solarwww.mtk.nao.ac.jp/wdc.html) for providing free access to the airglow data. UD and CJP are supported by the NSC of Taiwan through grant NSC 99-2111-M-008-006-MY2.

References

Barth, C. A., Three body reactions, *Ann. Geophys.*, **20**, 182–196, 1964.

Barth, C. A. and A. F. Hildebrandt, The 5577 A airglow emission mechanism, *J. Geophys. Res.*, **66**, 985–986, 1961.

Bendat, J. S. and A. G. Piersol, *Random Data: Analysis and Measurement Procedures*, 2nd ed., Wiley, New York, 1986.

Brenton, J. G. and S. M. Silverman, A study of the diurnal variations of the 5577 A [OI] airglow emission at selected IGY stations, *Planet. Space Sci.*, **18**, 641–653, 1970.

Cogger, L., R. Elphinstone, and J. Murphree, Temporal and latitudinal 5577 A airglow variations, *Can. J. Phys.*, **59**, 1296–1307, 1981.

Das, U. and H. S. S. Sinha, Long term variations in oxygen green line emission over Kiso, Japan from ground photometric observations using continuous wavelet transform, *J. Geophys. Res.*, **113**, D19115, doi:10.1029/2007JD009516, 2008.

Deutsch, K. A. and G. Hernandez, Long-term behavior of the OI 558 nm emission in the night sky and its aeronomical implications, *J. Geophys. Res.*, **108**, 1430, doi:10.1029/2002JA009611, 2003.

Donahue, T. M., B. Guenther, and R. J. Thomas, Distribution of atomic oxygen in the upper atmosphere deduced from Ogo 6 airglow observations, *J. Geophys. Res.*, **78**, 6662–6689, 1973.

Farge, M., Wavelet transforms and their applications to turbulence, *Ann. Rev. Fluid Mech.*, **24**, 395–457, 1992.

Fukuyama, K., Airglow variations and dynamics in the lower thermosphere and upper mesosphere—I. Diurnal variation and its seasonal dependency, *J. Atmos. Terr. Phys.*, **38**, 1279–1287, 1976.

Fukuyama, K., Airglow variations and dynamics in the lower thermosphere and upper mesosphere—II. Seasonal and long-term variations, *J. Atmos. Terr. Phys.*, **39**, 1–14, 1977.

Huang, N. E. and Z. Wu, A review on Hilbert-Huang transform: Method and its applications to geophysical studies, *Rev. Geophys.*, **46**, RG2006, doi:10.1029/2007RG000228, 2008.

Huang, N. E., Z. Shen, S. R. Long, M. C. Wu, H. H. Shih, Q. Zheng, N.-C. Yen, C. C. Tung, and H. H. Liu, The empirical mode decomposition and the Hilbert spectrum for nonlinear and non-stationary time series analysis, *Proc. R. Soc. Lond. A*, **454**, 903–995, 1998.

Liu, G. and G. G. Shepherd, An investigation of the solar cycle impact on the lower thermosphere O(^{1}S) nightglow emission as observed by WINDII/UARS, *Adv. Space Res.*, **42**, 933–938, doi:10.1016/j.asr.2007.10.008, 2008.

Liu, G., G. G. Shepherd, and R. G. Roble, Seasonal variations of the nighttime O(^{1}S) and OH airglow emission rates at mid-to-high latitudes in the context of the large-scale circulation, *J. Geophys. Res*, **113**, A06302, doi:10.1029/2007JA012854, 2008a.

Liu, G., G. G. Shepherd, and C. A. Tepley, Variations of the tropical O(^{1}S) nightglow as observed with the Arecibo Observatory photometer and WINDII on UARS, *J. Atmos. Sol. Terr. Phys.*, **70**, 1309–1317, doi:10.1016/j.jastp.2008.03.001, 2008b.

Nicolls, M. J., M. N. Vlasov, M. C. Kelley, and G. G. Shepherd, Discrepancy between the nighttime molecular ion composition given by the International Reference Ionosphere model and airglow measurements at low latitudes, *J. Geophys. Res.*, **111**, A03304, doi:10.1029/2005JA011216, 2006.

Rajesh, P. K., J. Y. Liu, H. S. S. Sinha, S. B. Banerjee, R. N. Misra, N. Dutt, and M. B. Dadhania, Observations of plasma depletions in 557.7-nm images over Kavalur, *J. Geophys. Res.*, **112**, A07307, doi:10.1029/2006JA012055, 2007.

Reid, I. M. and J. M. Woithe, The variability of 558 nm OI nightglow intensity measured over Adelaide, Australia, *Adv. Space Res.*, **39**, 1237–1247, 2007.

Shepherd, G. G., C. McLandress, and B. H. Solheim, Tidal in uence on O(^{1}S) airglow emission rate distributions at the geographic equator as observed by WINDII, *Geophys. Res. Lett.*, **22**, 275–278, 1995.

Shepherd, G. G., R. G. Roble, C. McLandress, and W. E. Ward, WINDII observations of the 558 nm emission in the lower thermosphere: The in uence of dynamics on composition, *J. Atmos. Sol. Terr. Phys.*, **59**, 655–667, 1997.

Shepherd, G. G., R. G. Roble, S.-P. Zhang, C. McLandress, and R. H. Wiens, Tidal in uence on midlatitude airglow: Comparison of satellite and ground-based observations with TIME-GCM predictions, *J. Geophys. Res.*, **103**, 14,741–14,751, 1998.

Shepherd, G. G., J. Stegman, P. Espy, C. McLandress, G. Thuillier, and R. H. Wiens, Springtime transition in lower thermospheric atomic oxygen, *J. Geophys. Res.*, **104**, 213–223, 1999.

Shepherd, G. G., G. Liu, and R. G. Roble, Large-scale circulation of atomic oxygen in the upper mesosphere and lower thermosphere, *Adv. Space Res.*, **35**, 1945–1950, 2005.

Shiokawa, K. and Y. Kiyama, A search for the springtime transition of lower thermospheric atomic oxygen using long-term midlatitude airglow data, *J. Atmos. Sol. Terr. Phys.*, **62**, 1215–1219, 2000.

Torrence, C. and G. P. Compo, A practical guide to wavelet analysis, *Bull. Am. Meteorol. Soc.*, **79**, 61–78, 1998.

Ward, W. E., A simple model of diurnal variations in the mesospheric oxygen nightglow, *Geophys. Res. Lett.*, **26**, 3565–3568, 1999.

Yee, J.-H., G. Crowley, R. G. Roble, W. R. Skinner, M. D. Burrage, and P. B. Hays, Global simulations and observations of O(^{1}S), $O_2(^1\Sigma)$ and OH mesospheric nightglow emissions, *J. Geophys. Res.*, **102**, 19,949–19,968, 1997.

U. Das (e-mail: umadas@jupiter.ss.ncu.edu.tw), C. J. Pan, and H. S. S. Sinha